Accepted July 29, 2017 to Computers & Structures

Truss optimization with buckling considerations using geometrically nonlinear beam modeling

Hazem Madah[1]*and Oded Amir[1]

[1] Faculty of Civil and Environmental Engineering, Technion - Israel Institute of Technology

1 Abstract

A unified approach that accounts for various buckling phenomena in truss design optimization is presented. Euler buckling of slender members, global buckling and stability of sequences of bars are all considered by optimizing the geometric nonlinear response instead of by imposing a large number of constraints. In the proposed approach, each truss member is modeled as a sequence of co-rotational beam elements with appropriate end-releases. By applying various imperfections, buckling of single truss members, unstable configurations and global buckling can be taken into account implicitly. A detailed discussion on key aspects of the proposed approach is presented, showing how the choice of imperfections highlights certain buckling types and leads to respectively stable designs. A comparison to other approaches and to results from the literature shows that the proposed approach can ensure local and global stability without actually imposing any buckling constraints. Finally, truss optimization for various levels of global deflections is presented, exposing the potential of the formulation for optimizing highly nonlinear responses.

Keywords: Truss optimization, geometric nonlinearity, buckling constraints.

2 Introduction

Structural engineers and architects are showing increasing interest in utilizing optimal structural forms due to their efficiency in transferring loads and their aesthetic shape. In the majority of cases, continuum-based topology optimization procedures are implemented, see for example Dombernowsky and Sondergaard (2009), Stromberg et al. (2012), Besserud et al. (2013) and Beghini et al. (2013). While continuum topology optimization is well-established (Bendsoe and Sigmund, 2003; Sigmund and Maute, 2013; Deaton and Grandhi, 2014), its direct applicability for contemporary construction practice is limited. In order to utilize structural forms generated by continuum procedures, they have to go through complicated conversion processes. This leads to complicated manufacturing of non-standard members and cross-sections that can be very expensive to construct. Therefore, some studies suggested methods to convert continuum topology forms to skeletal forms, for example (Mostafavi et al., 2013). Another approach will be to resort to the development of optimization approaches based on truss and frame modeling, which are very common in structural engineering. Then, the optimization procedures can yield designs that are directly manufacturable by standard structural members.

Additional motivation to studying trusses and frames is the interest in coupling robotic manufacturing with topology optimization, for accurate construction of complex forms. Robots can facilitate the construction of complicated forms that replace typical, repetitive forms. Then, better stiffness-to-weight ratios can be achieved, see for example Søndergaard et al. (2013) and Søndergaard et al. (2016).

In truss optimization, it is very common to use the ground structure approach, in which the design domain is divided into a grid of hinges and connected with assumed possible bars (see comprehensive review by Bendsoe and Sigmund, 2003, and references therein). The optimization problem can be solved by the classical linear programming (LP) formulation of minimum volume

*Corresponding author: *E-mail address:* hazem@technion.ac.il. *Full postal address:* Faculty of Civil and Environmental Engineering, Technion - Israel Institute of Technology, Haifa 32000, Israel

or weight under stress constraints, or it can be reformulated also with displacements and then solved by nonlinear programming (NLP) techniques.

The above mentioned classical formulations do not consider buckling, which encompasses various phenomena: Euler buckling of slender members; global buckling of the complete structure; and "chain" instability which is a particular artifact that results from the use of the ground structure approach. Therefore, optimized trusses obtained from the use of the classical formulations based on a ground structure may include compressed slender bars and unstable chains of bars, or may be vulnerable to global buckling. Dealing with buckling at the post-processing stage may lead to significant modifications of both the topology and the sizes of the optimized design. Therefore, buckling should be taken into account in the formulation, leading to different topologies and sizes compared to those obtained by standard truss optimization. The results of truss optimization that accounts for buckling will then be valid conceptual designs that will not require modifications when progressing to the detailed design stages. In this article, we focus exclusively on truss optimization following the ground structure approach due to its generality. Both local and global buckling have been considered in various studies using other parameterizations – for example in the context of latticed dome structures (Saka, 2007, 2009; Çarbas and Saka, 2009; Çarbas and Saka, 2012) and in the design of large-span three dimensional trusses (Pedersen, 2003).

Buckling in truss optimization is a classical topic and many studies have been carried out to impose it via different formulations. Global buckling has been imposed by adding a constraint on the positive semi-definiteness of the stiffness matrix (Ben-Tal et al., 2000; Kočvara, 2002) using a formulation based on semi-definite programming (SDP). Two solution methods have been suggested: one based on semi-definite approximations and the other on a quadratically constrained quadratic subproblem (QQP). It is important to note that such methods are not commonly used in structural optimization software and are still intended primarily for mathematical applications. Other studies accounted for global buckling by adding a constraint on the minimum buckling eigenvalue of trusses (Guo et al., 2005) and frames (Torii et al., 2015). In fact, Torii et al. (2015) used a similar model as in the current work – geometric nonlinear frame elements – to derive the geometric stiffness matrix and suggested that Euler buckling can be derived through buckling of a sequence of frame elements in a single bar.

Euler buckling of truss bars has been imposed, in the majority of cases, by adding an Euler buckling constraint on each bar (Rozvany, 1996; Zhou, 1996; Achtziger, 1999; Guo et al., 2001, 2005; Mela, 2014). This can increase significantly the number of constraint in the formulation, hence introducing difficulties in the computational solution when the ground structure consists of a large number of potential bars.

In classical formulations with stress constraints only, chain stability is not problematic because hinges can be canceled from the optimized layout without corrupting its optimality. However, in problems with Euler buckling constraints, hinge cancellation may lead to non-optimal solutions due to the change in member buckling length (Zhou, 1996). Therefore, Rozvany (1996) suggested to introduce geometrical imperfections to identify unstable chains, leading to the addition of a supporting bar to the chain in order to prevent its buckling, see also (Jalalpour et al., 2011; Descamps and Filomeno Coelho, 2014). Achtziger (1999) suggested a mathematical formulation that can identify and replace each chain of bars with a unified bar using a penalty approach based constraints. These constraints check if intermediate hinges of chains are connected to negligible bars, and according to their activity, the chain is replaced with unified bar. This formulation includes a sequence of linear and nonlinear constraints which have been solved using Sequential Linear Programming (SLP). (Mela, 2014) suggested a formulation based on mixed variable approach in which the discrete variables represent the existence of bars. To ensure chain stability, several linear constraints have been added to the formulation, that can identify chains if intermediate hinges of the chain are not connected to other bars. In addition, he assumed overlapping bars in the ground structure and added constraint to prevent the existence of overlapping bars in the optimized layout. Other studies adopted the addition of overlapping bars to the ground structure, where unstable chains were detected as global buckling using either SDP formulation (Kočvara, 2002) or EV formulation (Guo et al., 2001). (Tyas et al., 2006) suggested a formulation to stabilize compressed chains using a small perturbation loadings at hinges in different directions. These loads used to identify unstable compressed chains who stabilized later by braces or replaced with overlapping bars.

The aim of this work is to develop a truss optimization formulation that accounts for all buckling considerations in a single optimization problem, without any formal buckling constraints. In the

proposed approach, the truss members are modeled with geometric nonlinearity (GNL) using a co-rotational beam formulation. In the GNL model, each truss member is modeled as a sequence of co-rotational beam elements with moment releases only at hinged connections. By applying appropriate imperfections, buckling of single truss members and unstable configurations can be taken into account implicitly. The suggested procedure relies on geometric nonlinear analysis, meaning that it is more demanding in the analysis phase in comparison with existing approaches which are based on the linear-elastic response. Nevertheless, this added complexity is counter-balanced by the reduced complexity of the optimization problem, which involves only one global constraint. Therefore, the proposed approach can be very effective for problems with a large number of design variables. These arguments and further considerations will be discussed and presented in detail.

In the proposed procedure, the truss is optimized for end-compliance (Buhl et al., 2000), or equivalently for end load-bearing capacity when single load case is applied. Other studies proposed an eigenvalue based design sensitivity analysis for limit points or bifurcation points (Wu and Arora, 1988; Park and Choi, 1990; Kwon et al., 1999); and others proposed a continuum optimization procedure that optimizes for snap-through or bifurcation buckling loads (Lindgaard and Dahl, 2013). Instead of using eigenvalue analysis, Noguchi and Hisada (1993) suggested to approximate the eigenvectors by adding scaled displacements vectors as perturbations to the displacement vector. To reduce the imperfection sensitivity of the structure, (Kegl et al., 2008) proposed a 'worst-case' shape imperfection of shells using shape optimization in which the eigenvectors and eigenvalues are computed at each equilibrium point along the full nonlinear analysis. A similar procedure has been proposed by (Lindgaard et al., 2010) to find a 'worst-case' shape imperfection of composite shell structures when eigenvalue buckling is performed only at the load step before the limit point. This approach has been used later by (Lindgaard and Lund, 2011) in buckling optimization of composite structures using gradient-based algorithm. It is important to point out that in the current study, imperfections are assumed according to the initial design, meaning that the sensitivity to various imperfections is not accounted for explicitly. Another limitation is that gradients are derived only by the final load bearing capacity and final deformations at the prescribed displacement, so for statically indeterminate designs the compliance objective may not capture all internal buckling occurrences – however this was not encountered in any of the test cases.

The remainder of the article is organized as follows: First, the GNL beam element is reviewed briefly in Section 3, with particular emphasis on its utilization for capturing the buckling of truss bars. The proposed optimization problem formulation and the sensitivity analysis are presented in Section 4, followed by demonstrative examples based on graphical solutions and toy problems. Thereafter, the capability of the proposed approach to account for various buckling phenomena is demonstrated in Section 5 through benchmark examples from the literature. Finally, a summary and conclusions are given in Section 6.

3 Nonlinear beam modeling

Considering buckling within the optimization of truss structures requires the incorporation of three separate phenomena: Euler buckling of single members; global buckling of the whole structure; and chain stability, which is a bi-product of topology optimization based on the ground structure approach. In the proposed approach, the truss/frame members are modeled with geometric non-linearity using a co-rotational beam formulation. Then each type of buckling can be captured, in particular by using local imperfections of bars for inducing Euler buckling, and global imperfections of nodes' positions for inducing global buckling and chain instabilities. The main advantage of using the co-rotational beam element is in capturing buckling in the structural response, and then driving the design by optimization towards a buckling-resistant design. This approach replaces the need to impose numerous buckling constraints in the optimization problem formulation.

3.1 Co-rotational beam modeling

Local and global buckling can be traced in the structural model through geometric nonlinear analysis. In this study, a 2D co-rotational beam element is adopted (Wempner, 1969; Belytschko and Hsieh, 1973; Belytschko and Glaum, 1979). Its formulation is briefly presented hereunder, following the textbook representation by Crisfield (1991). Kinematic relations follow Kirchhoff's theory with large deformations, large rotations and small strains.

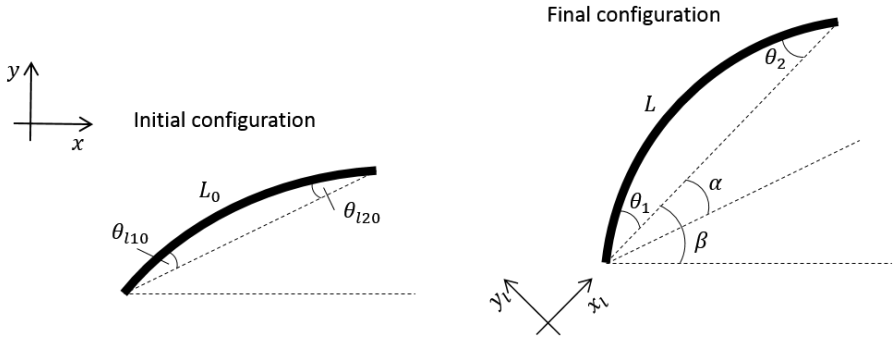

Figure 1: Co-rotational beam element

The internal loads vector $\mathbf{f}_{int}$ is given by

$$\mathbf{f}_{int} = \begin{bmatrix} -cN - \frac{sM_1}{L} - \frac{sM_2}{L} \\ -sN + \frac{cM_1}{L} + \frac{cM_2}{L} \\ M_1 \\ cN + \frac{sM1}{L} + \frac{sM_2}{L} \\ sN - \frac{cM_1}{L} - \frac{cM_2}{L} \\ M_2 \end{bmatrix} \tag{1}$$

where $c = cos(\beta)$ and $s = sin(\beta)$; β and L are the rotation and the length of the bar in the final configuration, see Fig. 1. The axial force and bending moments are given by

$$\begin{bmatrix} N \\ M_1 \\ M_2 \end{bmatrix} = \begin{bmatrix} \frac{EA}{L_0} & 0 & 0 \\ 0 & \frac{4EI}{L_0} & \frac{2EI}{L_0} \\ 0 & \frac{2EI}{L_0} & \frac{4EI}{L_0} \end{bmatrix} \begin{bmatrix} \Delta l \\ \theta_{l1} \\ \theta_{l2} \end{bmatrix} \quad , \quad \begin{bmatrix} \Delta l \\ \theta_{l1} \\ \theta_{l2} \end{bmatrix} = \begin{bmatrix} L - L_0 \\ \theta_1 - \alpha - \theta_{l10} \\ \theta_2 - \alpha - \theta_{l20} \end{bmatrix} \tag{2}$$

where L_0 is the initial length of the bar; α is the rigid body rotation; θ_i and θ_{li0} are the end-rotations of the bar in the final and the initial configurations, respectively. The full tangent stiffness matrix of a co-rotational beam element is given by

$$\mathbf{K}_t = \mathbf{B}^T\mathbf{C}\mathbf{B} + \frac{N}{L}\mathbf{z}\mathbf{z}^T + \frac{(M_1 + M_2)}{L^2}(\mathbf{r}\mathbf{z}^T + \mathbf{z}\mathbf{r}^T) \tag{3}$$

with

$$\mathbf{r} = [-c \quad -s \quad 0 \quad c \quad s \quad 0] \tag{4}$$

$$\mathbf{z} = [s \quad -c \quad 0 \quad -s \quad c \quad 0] \tag{5}$$

$$\mathbf{B} = \begin{bmatrix} -c & -s & 0 & c & s & 0 \\ -\frac{s}{L} & \frac{c}{L} & 1 & \frac{s}{L} & -\frac{c}{L} & 0 \\ -\frac{s}{L} & \frac{c}{L} & 0 & \frac{s}{L} & -\frac{c}{L} & 1 \end{bmatrix} \tag{6}$$

$$\mathbf{C} = \begin{bmatrix} \frac{EA}{L_0} & 0 & 0 \\ 0 & \frac{4EI}{L_0} & \frac{2EI}{L_0} \\ 0 & \frac{2EI}{L_0} & \frac{4EI}{L_0} \end{bmatrix} \tag{7}$$

where, in small deformations, the first term in Eq. (3) is the elastic stiffness matrix and the following terms form the geometric stiffness matrix.

Non-linear analysis is solved using a Newton-Raphson scheme under displacement control. The analysis system of equations takes the form

$$\mathbf{R}(\mathbf{u}) = \theta\hat{\mathbf{f}}_{ext} - \mathbf{f}_{int}(\mathbf{u}) \tag{8}$$

where $\mathbf{R}(\mathbf{u})$ is the vector of residual forces, θ is the load factor multiplying the constant external loads vector $\hat{\mathbf{f}}_{ext}$ and $\mathbf{f}_{int}$ is the internal forces vector. In displacement-controlled analysis, equilibrium is attained by choosing a prescribed displacement and solving for θ and $n-1$ unknown displacements, where n is the number of displacement degrees of freedom (DOF) in the model. As a result, a non-symmetric stiffness matrix is obtained and special treatment is required to keep it symmetric (Batoz and Dhatt, 1979), if this is desired due to computational considerations.

3.2 Capturing truss buckling with the GNL model

In this work, truss bars are modeled using at least two co-rotational beam elements with moment releases at hinged connections. Elements that are connected to hinges are modeled as fixed-hinge frame element while others are modeled as fixed-fixed elements. In order to avoid singularities at rotation degrees of freedom at hinges, in each hinge a single bar is connected rigidly. In addition, the geometric non-linear formulation is not sufficient for inducing buckling in the truss bars: it should be complemented with the imposition of various imperfections. In this section, we will demonstrate how the co-rotational model and the chosen imperfections are utilized for simulating various buckling phenomena in trusses.

In topology optimization of trusses, three types of buckling must be considered and for this purpose, various imperfection assumptions should be taken in the modeling stage. For example, Euler buckling in bars can be captured by perturbing the straightness of bars, whereas chain and global buckling can be captured if nodes are located with appropriate deviations from their "perfect" position. In the following examples, we illustrate and investigate the effect of various imperfections. In these test cases, it is assumed that all bars are made of solid circle cross-section and the modulus of elasticity is 10^6.

A demonstrative example of accounting for Euler buckling of a truss bar is illustrated in Fig. 2. The truss member consists of 20 co-rotational beam elements. The response of an imperfect bar is compared to an ideal one, and as can be seen, using the co-rotational beam element without any imperfection does not induce Euler buckling. On the other hand, taking a small imperfection of 0.1% is enough to prompt Euler buckling, yielding a force-displacement curve that clearly converges to the first buckling eigenvalue of the bar. In truss members, the direction of eccentricity is not important because the response is equivalent in both cases. However, the magnitude of the eccentricity affects the equilibrium path such that very low eccentricity can lead to an acute, highly nonlinear response that may hamper the convergence of Newton-Raphson iterations. In the context of truss optimization, local imperfections have been used before by Pedersen (2003) with an imperfection of 1%-2%, and by Pedersen and Nielsen (2003) who considered imperfections for calculating reduced stress limits.

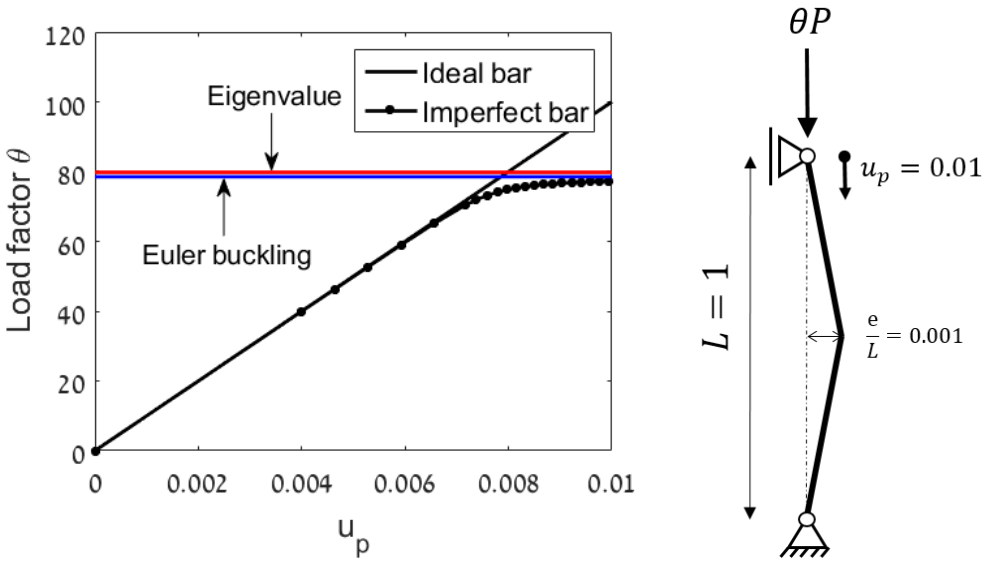

Figure 2: Euler buckling of a truss bar modeled by 20 co-rotational elements. With an eccentricity of 0.1%, the nonlinear response converges towards the buckling eigenvalue.

In this study, unstable chains are identified implicitly by the geometric nonlinear analysis, because a sequence of unbraced truss members will exhibit global buckling. The modeling of chain stability is investigated in the following example, which shows the important role of imperfections for identifying such unstable chains. The truss structure shown in Fig. 3 consists of a chain of two truss bars which are braced by another very thin bar at their hinged connection. In practice, a sequence of two compressed bars connected by a hinge without bracing is not stable, but it can be seen that it is computationally possible if the bars are perfectly aligned and connected without eccentricity. In this case, the very small stiffness of the bracing bar is enough to overcome singularity in the computational model, and the response of the two bars will be identical to the response of a single bar. In order to induce instability of the chain of bars, a small perturbation in the position of the hinge should be applied. This is enough to prompt buckling of the chain, which cannot be resisted by the very thin bracing – thus laying the foundations for a computational model that captures chain buckling directly via the response, alleviating the need for special constraints.

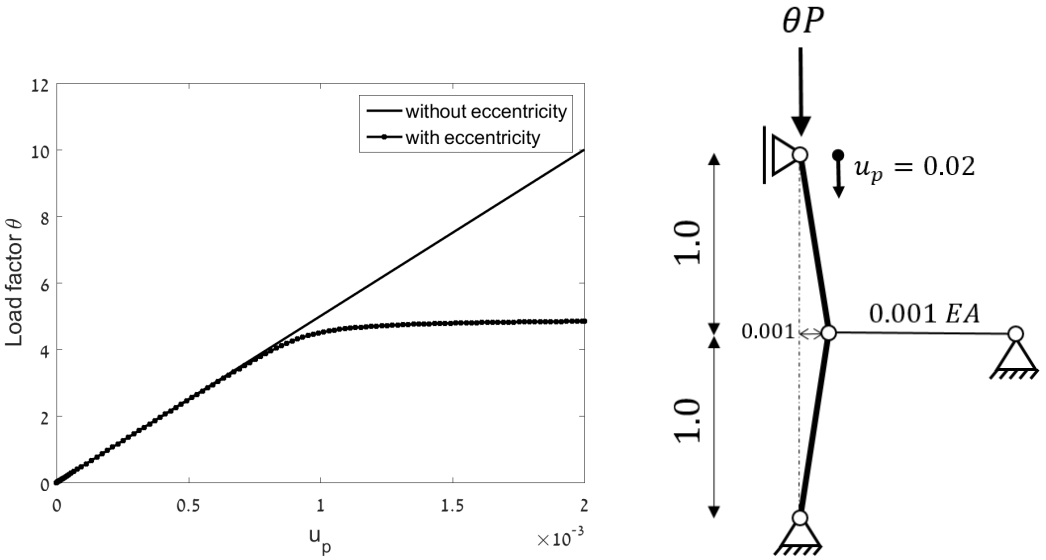

Figure 3: Demonstrative example of chain instability. The sequence of compressed bars exhibits buckling once the position of the hinge is slightly perturbed by a global imperfection.

It is important to clarify that if a negative imperfection is assumed, then the behavior will be different, i.e. the negligible bar will be tensioned and there will be no chain buckling. Clearly, choosing the imperfection shape of nodes' positions has a great effect on the total behavior of the structure. In this paper, imperfection shapes are assumed based on engineering judgment and future work will include a mechanism to define the appropriate shape of imperfection.

4 Optimization problem formulation

In this work we consider the classical problem of finding the stiffest structure with a given volume (weight) and vice-versa, with buckling taken into account implicitly by the nonlinear structural response. As buckling is accompanied with large deformations, we interpret "the stiffest structure" as the most buckling-resistant structure. In the case of displacement-controlled analysis and when the prescribed displacement is constant, the stiffest structure is obtained by maximizing the end-compliance, or equivalently, by maximizing the load bearing capacity if a single point load is applied. Therefore, the optimization problem takes the form

$$
\begin{aligned}
\min_{\mathbf{x}} \quad & f = -\theta \\
\text{s.t.:} \quad & g = \sum_{i=1}^{N} A_i \, l_i \leq V^*, \\
& 0 \leq x_i \leq 1 \qquad i = 1, ..., N \\
\text{with:} \quad & \mathbf{R}(\mathbf{x}, \mathbf{u}, \theta) = \theta \hat{\mathbf{f}}_{ext} - \mathbf{f}_{int}(\mathbf{x}, \mathbf{u}) = \mathbf{0}
\end{aligned} \tag{MaxF}
$$

where x_i is the design variable corresponding to the $i-$ truss bar; the bar cross section area is $A_i = A_{min} + (A_{max} - A_{min})x_i$, with A_{max} and A_{min} representing the given maximum and minimum cross-section areas; l_i is the bar length; V^* is the available volume; and N is the number of potential bars. In this formulation, the procedure starts with a relatively flexible structure (that satisfies the volume constraint) and converges towards the stiffest while maintaining the given volume. Therefore in some cases, intermediate structures may exhibit a highly non-linear response that will affect the procedure's convergence. To overcome this issue, a reversed formulation of minimum volume under a constraint on load bearing capacity constraint can be used:

$$
\begin{aligned}
\min_{\mathbf{x}} \quad & f = \sum_{i=1}^{N} A_i \, l_i \\
\text{s.t.:} \quad & g = \theta \geq \theta^* \\
& 0 \leq x_i \leq 1 \qquad i = 1, ..., N \\
\text{with:} \quad & \mathbf{R}(\mathbf{x}, \mathbf{u}, \theta) = \theta \hat{\mathbf{f}}_{ext} - \mathbf{f}_{int}(\mathbf{x}, \mathbf{u}) = \mathbf{0}
\end{aligned} \tag{MinV}
$$

where θ^* is the minimum load factor required. In this formulation, an initial conservative solution is assumed (i.e. with high volume), and then the procedure aims to minimize the volume while maintaining the required load bearing capacity. In both formulations the nested approach is utilized, meaning that the displacements $\mathbf{u}$ and the load factor θ are calculated separately outside the optimization problem. The design is then updated based on first-order gradients resulting from an adjoint sensitivity analysis. In the proposed formulations, moment of inertia of the cross-section can be expressed as function of the area using the relation $I = \alpha A^2$, where α relates to the shape of the cross-section, e.g. for solid circle cross-section $\alpha = 1/4\pi$ and for solid cubic cross-section $\alpha = 1/12$.

4.1 Demonstrative example: graphical solution

In order to provide initial insight regarding the application of the proposed approach, we examine a problem with two design variables that can be solved graphically. The solution can therefore be compared to the solution of a very common truss optimization formulation in the literature, i.e. minimum volume under Euler buckling constraints. The examined two-bar truss is made of solid circle cross-sections and the modulus of elasticity is 10^6, see Fig. 4a. In the formulation of minimum volume under Euler constraints, the truss is loaded by a point force of 50 at the top. By examining different combinations of cross-section areas, the axial forces in each bar are calculated and the buckling constraints are plotted in Fig. 4b. In a sizing optimization problem, the feasible region must satisfy both constraints hence the optimal solution is attained at $(A_1, A_2) = (0.0066, 0.0046)$ with a minimum volume of $V = 0.0103$. If topology optimization is the goal, then the objective can be further reduced by eliminating bars, leading to singular points in the feasible region. In this example, such a singular optimum is attained at $(A_1, A_2) = (0, 0.0076)$ with a minimum volume of 0.006545. It is important to clarify that arriving to singular optima by numerical search algorithms might be difficult or even impossible (e.g. Kirsch, 1990).

For solving the formulation (MaxF) graphically, a prescribed displacement of $u_p = 0.01$ is applied in the direction of the load and a local imperfection $e/L = 0.001$ is introduced to initiate Euler buckling of the bars. Then the load factor is calculated and plotted in Fig. 4c through different combinations of cross-section areas. Taking the optimal volume of 0.006545 as a constraint and maximizing the load factor leads to the same solution $(A_1, A_2) = (0, 0.0076)$ with an objective value of $\theta = 50$. Similarly, the graphical solution of formulation (MinV) is illustrated in Fig. 4d, where

the required load factor is given as $\theta = 50$. The minimum volume which satisfies the constraint is attained also at the precise same solution as before. This example shows that the proposed approach can, in some cases, mimic the straightforward formulation of minimum volume subject to buckling constraints, without actually imposing buckling constraints. In addition, the issues of singular optima and discontinuous feasible regions can be overcome, as can be seen in Fig. 4c,d. It is important to point out that the two-bar example is relatively simple and the observations may not be valid for more complicated structures, see Sec. 5 for a discussion on accounting for buckling in benchmark examples. At the same time, we believe that the graphical solutions reveal the potential of the proposed approach and encourage its investigation.

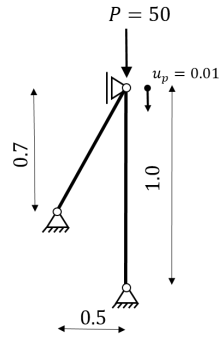

(a) Truss structure

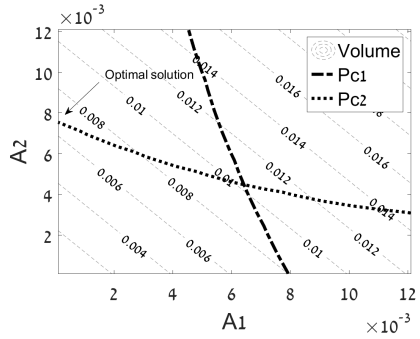

(b) Graphical solution using formulation of minimum volume under Euler constraints

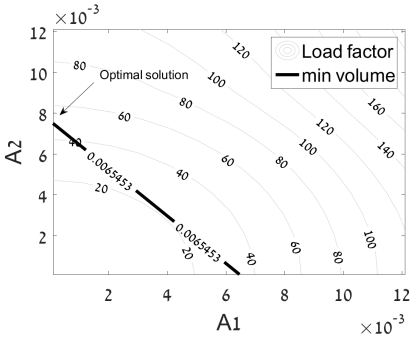

(c) Graphical solution using (MaxF) formulation

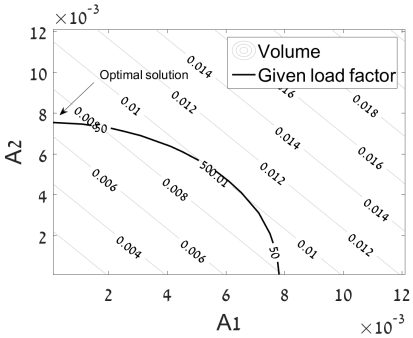

(d) Graphical solution using (MinV) formulation

Figure 4: Graphical solution of two bar truss

4.2 Sensitivity analysis

All numerical solutions of the optimization problems in this study were obtained with the Method of Moving Asymptotes (MMA, (Svanberg, 1987)) a first-order gradient-based algorithm. In this section, we derive the gradients of the objective and constraint in the two formulations, (MaxF) and (MinV). Sensitivity analysis for problems that involve large deformations depends on the final equilibrium only and disregards the solution path. For the formulation (MaxF) using displacement-controlled analysis, the augmented objective is

$$\hat{f}(\theta, \mathbf{x}, \mathbf{u}) = f(\theta, \mathbf{x}, \mathbf{u}) - \lambda^T [\theta \hat{\mathbf{f}}_{ext} - \mathbf{f}_{int}(\mathbf{x}, \mathbf{u})] \tag{9}$$

Differentiation with respect to a certain design variable gives

$$\frac{\partial \hat{f}}{\partial x_i} = \frac{\partial f}{\partial x_i} + (\frac{\partial f}{\partial \mathbf{u}} + \lambda^T \frac{\partial \mathbf{f}_{int}}{\partial \mathbf{u}}) \frac{\partial \mathbf{u}}{\partial x_i} + (\frac{\partial f}{\partial \theta} - \lambda^T \hat{\mathbf{f}}_{ext}) \frac{\partial \theta}{\partial x_i} + \lambda^T \frac{\partial \mathbf{f}_{int}}{\partial x_i} \tag{10}$$

where, without loss of generality, we assumed that the external forces do not depend upon the design.

The derivatives $\frac{\partial f}{\partial x_i} = 0$, $\frac{\partial f}{\partial \mathbf{u}} = \mathbf{0}$ and $\frac{\partial f}{\partial \theta} = -1$ are found straightforwardly from the definition of the objective, whereas $\frac{\partial \mathbf{f}_{int}}{\partial \mathbf{x}}$ are explicit derivatives of the co-rotational model

$$\frac{\partial \mathbf{f}_{int}^{i}}{\partial x_i} = \begin{bmatrix} -\frac{E(A_{max}-A_{min})(cL(L-L_0)+12s\alpha A_i(\theta_{l1}+\theta_{l2})}{LL_0} \\ \frac{E(A_{max}-A_{min})(-sL(L-L_0)+12c\alpha A_i(\theta_{l1}+\theta_{l2})}{LL_0} \\ \frac{4\alpha E(A_{max}-A_{min})A_i(2\theta_{l1}+\theta_{l2})}{L_0} \\ \frac{E(A_{max}-A_{min})(cL(L-L_0)+12s\alpha A_i(\theta_{l1}+\theta_{l2})}{LL_0} \\ -\frac{E(A_{max}-A_{min})(-sL(L-L_0)+12c\alpha A_i(\theta_{l1}+\theta_{l2})}{LL_0} \\ \frac{4\alpha E(A_{max}-A_{min})A_i(\theta_{l1}+2\theta_{l2})}{L_0} \end{bmatrix} \tag{11}$$

where $A_i = A_{min} + (A_{max} - A_{min})x_i$.

The definition of the tangent stiffness matrix corresponding to the final equilibrium point gives $\frac{\partial \mathbf{f}_{int}}{\partial \mathbf{u}} = \mathbf{K}$. In contrast, $\frac{\partial \mathbf{u}}{\partial x_i}$ and $\frac{\partial \theta}{\partial x_i}$ cannot be calculated explicitly hence the following coupled system of adjoint equations needs to be solved

$$\begin{aligned} \frac{\partial f}{\partial \mathbf{u}} + \lambda^T \frac{\partial \mathbf{f}_{int}}{\partial \mathbf{u}} = 0 \\ \frac{\partial f}{\partial \theta} - \lambda^T \hat{\mathbf{f}}_{ext} = 0 \end{aligned} \tag{12}$$

Inserting the known derivatives to the set of equations (12) and utilizing the subscripts p and f to denote the prescribed and non-prescribed DOF, the set of equations can be represented as follows

$$\begin{bmatrix} \mathbf{K}_{ff} & \mathbf{K}_{fp} \\ \hat{\mathbf{f}}_{ext}^{f} & \hat{\mathbf{f}}_{ext}^{p} \end{bmatrix} \begin{pmatrix} \boldsymbol{\lambda}_f \\ \lambda_p \end{pmatrix} = \begin{pmatrix} \mathbf{0} \\ -1 \end{pmatrix} \tag{13}$$

Finally, the solution for $\boldsymbol{\lambda}$ is inserted back into (10) to give the design sensitivities of the load-bearing capacity

$$\frac{\partial \hat{f}}{\partial x_i} = \lambda^T \frac{\partial \mathbf{f}_{int}}{\partial x_i} \tag{14}$$

The sensitivity of the volume constraint can be derived straightforwardly

$$\frac{\partial g}{\partial x_i} = (A_{max} - A_{min}) l_i \tag{15}$$

For the problem of (MinV), the objective and constraint are simply interchanged so the same sensitivity analysis can be utilized.

4.3 The effect of various imperfections

In this section, the influence of imposing various imperfections is investigated and examined on the classical truss problem shown in Fig. 5. The purpose of this investigation is to examine the capability of the formulation to capture the various buckling phenomena that occur in truss optimization. The structure is loaded at the bottom right side of the design domain, and the prescribed displacement is chosen in the same DOF. The ground structure is shown in Fig. 5b. As it can be seen, it includes two overlapping bars that can replace a chain of two bars. Local and global imperfections are sketched in Fig. 5c and Fig. 5d, respectively. The global imperfection shape is chosen according to the curvature of the loaded edge of the cantilever beam. Similar results were obtained by choosing the deformed shape of the truss, following a linear analysis, as the global imperfection. The bars are made of solid circle cross-section and the optimization is solved using MMA with the parameters given in Table 1.

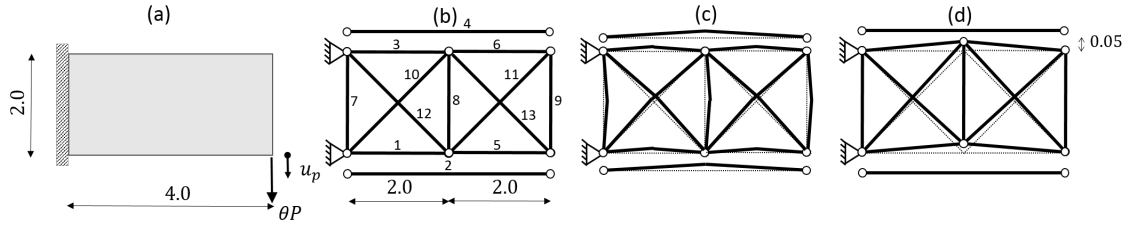

Figure 5: (a) design domain; (b) ground structure; (c) local imperfections $e/l = 0.01$; (d) nodes positions imperfection

Table 1: Solution parameters for 11-bar truss example

Parameter	Value
A_{max}	$2 \cdot 10^{-3}$
A_{min}	$2 \cdot 10^{-7}$
V^*	$1 \cdot 10^{-2}$
E	$1 \cdot 10^{6}$
MMA move limit	$1 \cdot 10^{-2}$

Various optimized designs are generated by solving formulation (MaxF) with different combinations of imperfections and prescribed displacement. In the following comparison, the effects of local and global imperfections will be examined under two scales of deflections: small deflections of $u_p = 1 \cdot 10^{-6}$ and large deflections of $u_p = 1 \cdot 10^{-2}$. Our comparison focuses on six particular layouts obtained from different combinations of imperfections which are listed in Table 2, while the optimized layouts are shown in Fig. 6. In these layouts, bars with cross-section area smaller than $1 \cdot 10^{-4}$ times the maximum cross-section area are assumed negligible and are not displayed.

Table 2: Effect of various imperfection on optimal design.

Layout	Imperfection assumed			Response(layout 1 imp.)		Response(layout 6 imp.)	
	local	global	u_p	$\theta(u_p = 10^{-6})$	$\theta(u_p = 10^{-2})$	$\theta(u_p = 10^{-6})$	$\theta(u_p = 10^{-2})$
1	without	without	10^{-6}	$3.906 \cdot 10^{-5}$	$3.395 \cdot 10^{-1}$	$3.532 \cdot 10^{-6}$	$0.592 \cdot 10^{-2}$
2	with	without	10^{-6}	$3.846 \cdot 10^{-5}$	$0.161 \cdot 10^{-1}$	$8.257 \cdot 10^{-11}$	$1.434 \cdot 10^{-8}$
3	without	with	10^{-6}	$3.879 \cdot 10^{-5}$	$3.884 \cdot 10^{-1}$	$6.437 \cdot 10^{-6}$	$1.606 \cdot 10^{-2}$
4	with	with	10^{-6}	$3.753 \cdot 10^{-5}$	$3.757 \cdot 10^{-1}$	$9.498 \cdot 10^{-6}$	$8.992 \cdot 10^{-2}$
5	with	without	10^{-2}	$2.114 \cdot 10^{-5}$	$2.112 \cdot 10^{-1}$	$2.563 \cdot 10^{-6}$	$10.95 \cdot 10^{-2}$
6	with	with	10^{-2}	$2.101 \cdot 10^{-5}$	$2.099 \cdot 10^{-1}$	$2.531 \cdot 10^{-6}$	$10.95 \cdot 10^{-2}$

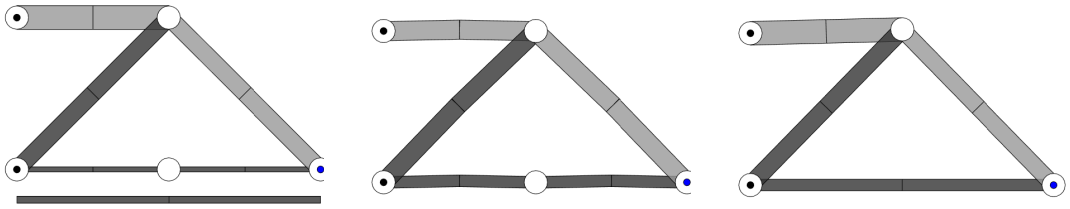

(a) Layout (1) (b) Layout (2) (c) Layout (3)

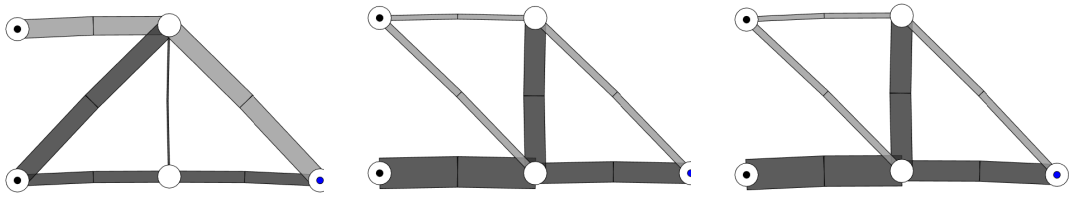

(d) Layout (4) (e) Layout (5) (f) Layout (6)

Figure 6: Different layouts of 11-bar truss.

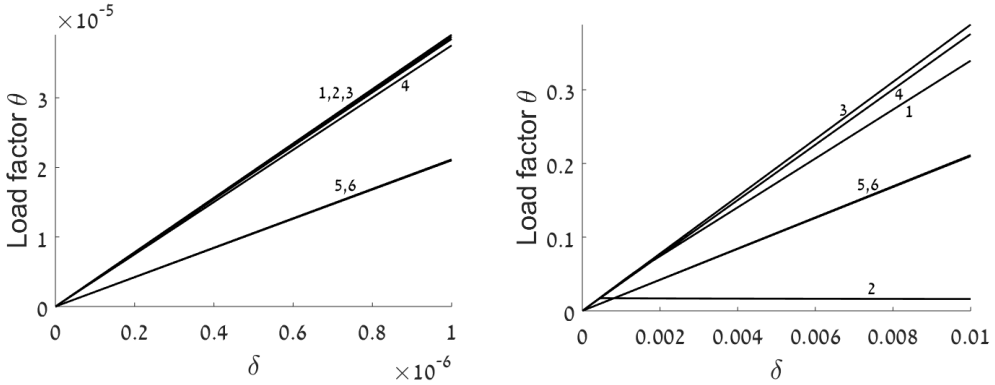

Figure 7: Full response curves over the imperfections for which layout 1 is obtained: (a) small deflections, $u_p = 10^{-6}$; (b) large deflections, $u_p = 10^{-2}$. Under infinitesimal deflections, layouts 1, 2, 3 and 4 are dominant over layouts 5 and 6, as expected. Once large deflections are prescribed, layout 2 buckles due to the hinged chain.

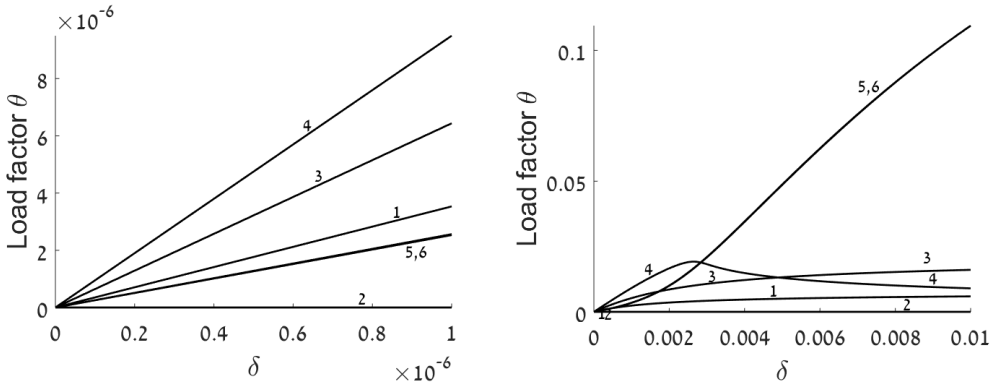

Figure 8: Full response curves over the imperfections for which layout 6 is obtained: (a) small deflections, $u_p = 10^{-6}$; (b) large deflections, $u_p = 10^{-2}$. Under infinitesimal deflections, layout 4 is dominant whereas layout 2 collapses due to the unbraced hinge. Once large deflections are prescribed, only layouts 5 and 6 maintain their structural integrity.

From layout 1 (Fig. 6a) it can be observed that applying no imperfections can lead to the optimal design of the well-known plastic design problem of minimum volume subject to stress constraints, where the bottom bar has the same cross-section area as the sum of cross-section areas of overlapping bars. Assuming local imperfection (Fig. 6b) leads to practically the same layout but without the overlapping bar that buckles locally – meaning that the procedure successfully detected Euler buckling of a long and slender bar and removed it, while an unstable chain of two short bars had been kept because no imperfections were applied to it. Assuming global imperfections only leads to the opposite design choice where chain buckling was detected, as can be seen in the layout of Fig. 6c. The sequence of the two short bars has been removed in the optimization procedure and the long slender bar was kept maintained. When prescribing large deformations, two similar layouts are obtained by assuming either local imperfections only or local and global imperfections, see Fig. 6d,e. In this case, global imperfections do not affect the optimal design because they are obtained implicitly by the large deformations of the truss. The layouts show clear preference towards buckling-safe tensile forces, where the compressed bars are much shorter than in layouts 1-3.

For further insight regarding the influence of the various imperfections, we present load-displacement curves of the five layouts, see Fig. 7 and Fig. 8. These curves are computed under the imperfection assumptions of layouts 1 and 6 and in two ranges of prescribed deflections. With no imperfections, layouts 1, 2, 3 and 4 exhibit almost identical responses under small deflections (Fig. 7a), whereas under large deflections (7b), layouts 1, 3 and 4 are the stiffest and layout 2 buckled. Chain buckling of layout 2 resulted from the development of large displacements and rotations of the truss. In both deflections scales, layouts 5 and 6 were stable but not the stiffest, as expected. With local and global imperfections assumed and a large prescribed deflection, it can be seen in Fig. 8b that the layouts 5 and 6 can sustain the highest loads, as expected because they were designed with such imperfection. When examining the response under a very small prescribed deflection (Fig. 8a), layout 2 is unstable due to the unbraced chain and the stiffest solution is layout 4. Once the prescribed displacement is increased then layouts 1, 3 and 4 buckle, and when u_p exceeds $2.5 \cdot 10^{-3}$ only layouts 5 and 6 maintain their structural integrity.

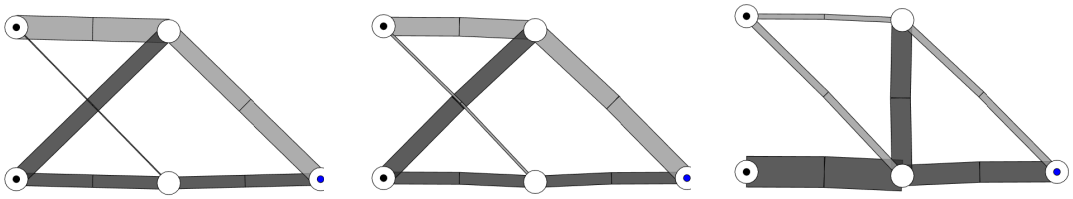

(a) Layout (3*) (b) Layout (4*) (c) Layout (6*)

Figure 9: Layouts 3, 4 and 6 over inverted global imperfection (-0.05)

In order to investigate the effect of the direction of imperfections, a series of numerical studies were performed on the same example as in Fig. 5 over inverted directions of local and global imperfections. The results were then compared to results listed in Table 2 and to the layouts in Fig. 6. Assuming an inverted direction of local imperfection does not affect the results, as expected. This is also discussed in Section 3.2. However, inverting the direction of global imperfections may lead to remarkable differences in the optimized design. This is demonstrated in Fig. 9 where layouts 3^* and 4^* are different than their counterparts, layouts 3 and 4 in Fig. 6. As it can be seen, the bottom bar in layout 3 was replaced in layout 3^* with a braced chain and the compressed bracing bar in layout 4 was replaced with a tensioned diagonal bracing bar in layout 4^*. Practically, global imperfections can result from the structural deformations or from construction deviations whose directions are difficult to predict. Therefore in order to achieve robust optimized design, global imperfection directions must be assumed in the most critical pattern. Comparing results over the different directions of the global imperfections shows that layouts 3 and 4 are more robust than 3^* and 4^* due to the tensioned bracing that may buckle when the imperfection is inverted. From the other hand, layout 3 is not affected and the bracing bar in layout 4 will be in tension instead of in compression. This can shed light on the importance of choosing the shape of global imperfection, which must be assumed to give the most robust design. Global imperfection shape in layouts 3 and 4 is upwards and it resembles the curvature shape of an edge loaded cantilever beam that coincides with the approach proposed by Noguchi and Hisada (1993) where imperfection is applied based on the displacements of the structure. In the current study, magnitudes of imperfections were chosen to be large enough such that all buckling phenomena are exposed. A more general approach will be investigated thoroughly in future work.

In conclusion, based on the demonstrative example above, the influence of various imperfection assumptions in truss optimization is evident. Local imperfections are necessary for capturing the slenderness and buckling of single members, while global imperfections are essential to ensure the global stability of the structure including the chains. Finally, the magnitude of the prescribed displacement affects the range of deformation for which the optimized design is indeed dominant over other designs. The magnitudes of imperfections and the shape of the imperfection in terms of nodes' positions, affect the robustness of the optimized design and should be chosen according to the specific case and design target, e.g. according to deformation shape or curvature of the structure. In principle, the suggested approach is general and can capture all buckling phenomena that can occur in truss optimization based on ground structures. Nevertheless, in the examples presented in Section 5, the imperfections were set according to the nature of the ground structure and to the specific buckling phenomenon which was investigated in the literature.

4.4 Aggregated stress constraints

In some cases, for generating viable optimized trusses and for the sake of a fair comparison to the literature, it is necessary to enrich the formulations (MaxF) and (MinV) with additional

considerations. In particular, stress constraints will be briefly reviewed in this section, and later utilized in some of the examples. In principle, in order to account for stresses in the truss bars, a stress constraint on each bar should be added to the formulation. In the current work, for reducing the number of constraints, all stress constraints are aggregated into a single global stress constraint that is formulated using the widely used p-norm function that takes the form (e.g. Haftka and Gürdal, 2012):

$$g(\theta, \mathbf{u}, \mathbf{x}) = \left\| \frac{\boldsymbol{\sigma}}{\sigma_y} \right\|_p - 1 \leq 0 \tag{16}$$

where $\boldsymbol{\sigma}$ is the vector of normal stresses in the bars, measured in their neutral axes; σ_y is the allowable given stress; and p is the p-norm factor. Eq. (16) can be presented explicitly as

$$g(\theta, \mathbf{u}, \mathbf{x}) = \sqrt[p]{\sum_{i=1}^{N_b} \left(\frac{\sigma_i}{\sigma_y} \right)^p} - 1 \leq 0 \tag{17}$$

where N_b is the number of bars and σ_i is the normal stress in the i-th bar. Because in the current work truss bars are divided into two or more co-rotational elements, similar stresses are computed in adjacent finite elements and this may introduce difficulties in using a global stress constraint. To overcome these difficulties, Eq. (17) can be expressed as

$$g(\theta, \mathbf{u}, \mathbf{x}) = \sqrt[p]{\sum_{i=1}^{N_b} \sum_{j=1}^{N_e} \left(\frac{{}^j\sigma_i}{\sigma_y} \right)^p} - 1 \leq 0 \tag{18}$$

where for relatively small p factor, computing with similar stresses in the same bar may overestimate the actual maximum stress. Hence in order to measure the exact stress in the bar, the sum of the stresses in the same bar is divided by N_e, the number of elements composing the bar, giving

$$g(\theta, \mathbf{u}, \mathbf{x}) = \sqrt[p]{\frac{1}{N_e} \sum_{i=1}^{N_b} \sum_{j=1}^{N_e} \left(\frac{{}^j\sigma_i}{\sigma_y} \right)^p} - 1 \leq 0 \tag{19}$$

The gradient of the stress constraint is derived using adjoint method, in a similar manner as for the load-carrying functional. Derivatives with respect to the design variables are

$$\frac{\partial g}{\partial x_i} = \lambda^T \frac{\partial \mathbf{f}_{int}}{\partial x_i}. \tag{20}$$

The adjoint vector λ is the solution of the following set of equations:

$$\begin{bmatrix} \mathbf{K}_{ff} & \mathbf{K}_{fp} \\ \hat{\mathbf{f}}_{ext}^f & \hat{f}_{ext}^p \end{bmatrix} \begin{pmatrix} \boldsymbol{\lambda}_f \\ \lambda_p \end{pmatrix} = \begin{pmatrix} -B^T \frac{\partial g}{\partial \boldsymbol{\sigma}} E \\ 0 \end{pmatrix} \tag{21}$$

where $B = \frac{\partial \epsilon}{\partial u}$ and $\frac{\partial g}{\partial \boldsymbol{\sigma}}$ can be evaluated explicitly based on the co-rotational model and on Eq. (19). In the p-norm formulation, the accuracy of the approximation of the maximum stress in the bars depends on the p factor, where an infinite value leads to the exact maximum stress. On the other hand, increasing p introduces high nonlinearities and may cause difficulties in computing the gradients, hence a good balance between the accuracy and stability of the optimization should be obtained.

5 Examples

In this section, we demonstrate the capabilities of the proposed approach to account for various buckling phenomena occuring in truss optimization. First, we examine the procedure by direct comparison to two well-known results from the literature, namely global buckling of a compressed 2D tower by Ben-Tal et al. (2000) and Euler buckling and chain stability of a cantilever by Achtziger (1999). Finally, an additional example is presented that demonstrates the versatility of the approach in optimizing for various ranges of deformation. When comparing to results from the

literature, it is in some cases difficult to provide a direct quantitative comparison using the limited data supplied in literature, hence only qualitative comparison has been pursued.

In all examples, we assume that all bars are made of solid circle cross-sections, and that the modulus of elasticity is 10^6.

Stopping criterion in the following examples is established according to the last design variable update, when the error of the $i-$th iteration ε_i gets below a required error ε in such

$$\varepsilon_i = \frac{max(|\mathbf{x}_i - \mathbf{x}_{i-1}|)}{max(|\mathbf{x}_i|)} \tag{22}$$

5.1 Global buckling

In this example, the proposed formulation is applied on a case that involves global buckling. Therefore, only global imperfections have been applied and no overlapping bars were modeled in the ground structure. Comparison to results from the literature centers on the example of Ben-Tal's compressed tower (Ben-Tal et al., 2000) and the aim is to mimic the results from the reference using the current approach. The geometry, ground structure, applied load and prescribed deformation are shown in Fig. 10a. The global imperfection is derived from the bending deformation of the initial truss under a concentrated load, also matching the first buckling mode, see Fig. 10b. The prescribed displacement is $u_p = 0.01$ and is chosen to be in direction of the first buckling mode which is, in this example, perpendicular to the direction of the applied load.

The total number of potential bars is 43 and each bar is divided into two co-rotational beam elements, giving 186 analysis DOF. The aim is to achieve identical buckling resistance in both directions of the tower, hence it is assumed that the columns and struts are symmetric. Consequently, the number of design variables for optimization is 24. The solution was achieved using formulation (MaxF) with a given volume of $V^* = 0.01$. The optimization problem is solved using MMA with the parameters: $A_{max} = 1.0 \cdot 10^{-3}$; $A_{min} = 1.0 \cdot 10^{-5}$; an external move limit of 0.1; and required error $\varepsilon = 1.0 \cdot 10^{-4}$.

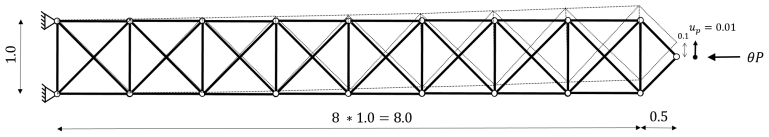

(a) Ground structure

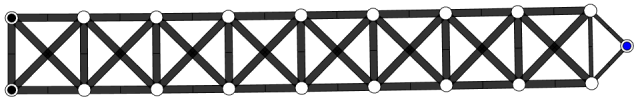

(b) Deformation shape of initial ground structure

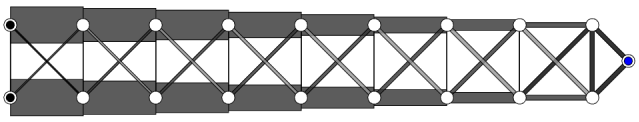

(c) Optimized layout - proposed formulation

Figure 10: Truss optimization accounting for global buckling – design of a compressed tower following Ben-Tal et al. (2000).

The initial truss has uniform cross-sections of $2.04 \cdot 10^{-4}$, chosen so to satisfy the volume constraint. The initial load-bearing capacity is 0.323. Within 22 design iterations, optimization leads to the optimized design with a load-bearing capacity of 0.9705. The optimized layout is shown in Fig. 10c, and it clearly resembles the result from the literature, which was achieved by semi-definite programming. The optimized design has tapered columns that have bigger cross-

section areas close to the supports, while the internal struts are flexible near the supports and stiffer near the loaded edge.

Full response curves of intermediate designs are shown in Fig. 11. It can be seen that the initial response is nonlinear, and during optimization the response approaches a linear curve and simultaneously the load bearing increases. Qualitatively, a comparison between results of the proposed procedure and the literature (in particular, see (Ben-Tal et al., 2000) Figure 4d) shows that similar layouts have been obtained in both formulations. This indicates that the proposed formulation is capable of imposing constraints on global buckling in truss optimization, without an actual constraint in the form of an eigenvalue or positive semi-definiteness requirement.

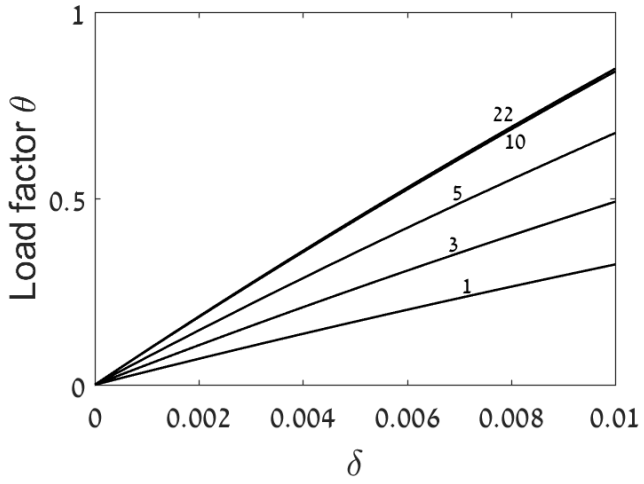

Figure 11: Truss optimization accounting for global buckling – full response curves of designs corresponding to selected optimization iterations. The initial response is nonlinear, and during optimization the response approaches a linear curve while the load bearing increases.

5.2 Euler buckling and chain stability

In this example, we show how local stability can be accounted for in truss topology optimization. As a basis for investigation, the bending truss structure by Achtziger (1999) is chosen. In the referenced article, the author proposes a sequential approach that can capture both Euler buckling of slender members and chain stability. In order to capture chain instability and overcome it in the optimization, overlapping bars are added to the ground structure and global imperfections are applied. The imperfections consist of an upwards vertical camber of 0.2 which is applied on the whole ground structure, while joints in the middle row are perturbed horizontally by a 0.025 imperfection.

The geometry of the ground structure, the applied load and the prescribed deformation are shown in Fig. 12a. The total number of design variables, each representing a potential bar, is 172 and each bar is divided into two co-rotational beam elements, giving 615 analysis DOF. In this case we implement formulation (MinV) that minimizes volume with a required load bearing capacity of $\theta^* = 1$. In addition, we impose a global p-norm stress constraint in order to obtain a fair comparison to the results in the reference which included stress constraints. The allowable stress limit is $\sigma_y = 1000$ and the p-norm factor is $p = 50$. The optimization problem is solved using MMA, with the parameters $A_{max} = 0.01$ and $A_{min} = 1.0 \cdot 10^{-6}$, which represent a more "topological" design intent compared to the previous example. As the ground structure consists of many potential chains which can be braced and stabilized with very thin bars, it was difficult to obtain a clear solution using a constant move limit on the design variables. A constant move limit of 0.01 was found to be too coarse for such braces that can alternately enter and exit the design solution and cause acute differences in the nonlinear response. Therefore, an adaptive technique is used in which the move limit is computed as a percentage of the last design variable update by MMA. In this way, modifications of both small and large cross-sections are bounded relatively to their current cross section and not by an absolute value. In this example, a move limit of 10% is used. This technique assists in stabilizing the convergence of the optimization process and in

avoiding acute nonlinear responses. The disadvantage is the need to perform a large number of design iterations in order to completely remove bars from the design.

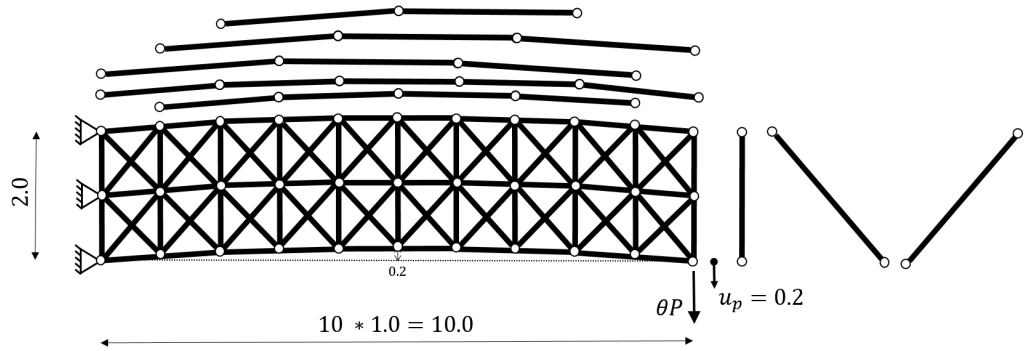

(a) Ground structure

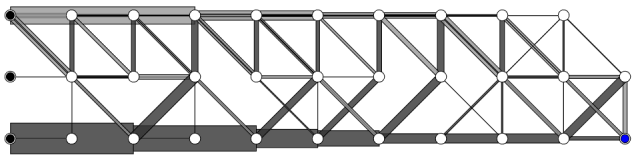

(b) Optimized design by the proposed formulation

Figure 12: Truss topology optimization accounting for Euler buckling and chains – design of a cantilever following Achtziger (1999).

A conservative initial truss is assumed with uniform cross-section areas of 0.0045 and a total volume of 1.385. This truss has load-bearing capacity of 8.483 and the aggregated maximum stress is 5422. For stopping criterion the required error of $\varepsilon = 1.0 \cdot 10^{-5}$ was chosen, and bars with cross-section area less than 0.15% of the maximum bar are assumed negligible and not shown in the optimized layout. The optimized design with a volume 0.09 is attained in 6576 design iterations. A clear topological solution is attained in less than 2000 design iterations, and further iterations are needed in order to remove both overlapping bars and bars with negligible cross-section. The optimized design is shown in Fig. 12b and intermediate layouts found after 100, 1000, 2000, 4000 design iterations are shown in Fig. 13.

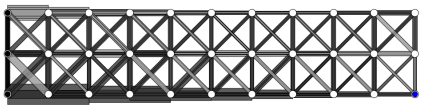

(a) Layout in iteration no. 100, V=0.1907

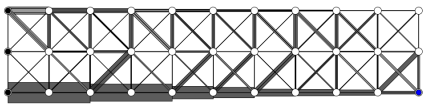

(b) Layout in iteration no. 1000, V=0.0996

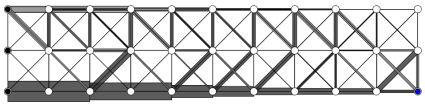

(c) Layout in iteration no. 2000, V=0.0939

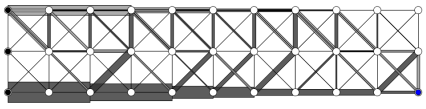

(d) Layout in iteration no. 4000, V=0.0911

Figure 13: Truss topology optimization accounting for Euler buckling and chains – intermediate designs.

Examining the result, it can be seen that overlapping tensioned bars still exist in optimized design, but compressed ones do not. Cross-section areas of compressed bars close to the support are chosen according to the stress constraint, therefore the procedure preferred slender overlapping bars over braced chains. In contrast, near the loaded edge, overlapping compressed bars are too slender and sensitive to buckling, therefore a braced chain was preferred. It can be seen that the optimized design obtained with the proposed procedure is different from that presented in the literature with the same ground structure. In fact, it will be shown that the current result is

presumably a better optimum.

In order to perform a direct comparison to the literature, the same problem is solved again but with a coarse ground structure. The geometry of the coarse ground structure, the applied load and the prescribed deformation are shown in Fig. 14a. The total number of potential bars is 34 and each bar is divided to two co-rotational beam elements, giving 138 analysis DOF. The optimized design reaches a volume of 0.1077 and is attained after 1232 design iterations. It is displayed in Fig. 14b and it clearly resembles the layout obtained in the literature (see (Achtziger, 1999) Fig. 1c) where negligible bars with cross-section area less than 1% of the maximum bar are not shown in the optimized layout. A quantitative comparison of the results with both fine and coarse ground structures shows that using the fine ground structure leads to an objective value 16% lower than that of the coarse structure. Euler buckling of compressed members of the optimized layouts were examined for the required load bearing capacity and it is found that they are all imposed. This demonstrates the capability to deal with design problems that involve both Euler buckling and chain stability, just by using a geometrically nonlinear model that can capture all buckling modes so that they are implicitly accounted for in the optimization.

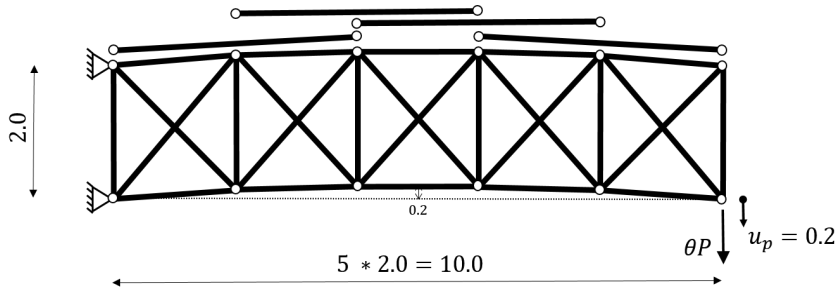

(a) Coarse ground structure

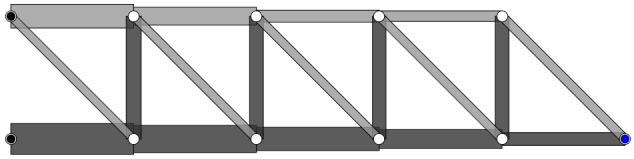

(b) Optimized design with a coarse ground structure

Figure 14: Truss topology optimization accounting for Euler buckling and chains – design of a cantilever following Achtziger (1999), with a coarse ground structure.

5.3 Optimizing for various global prescribed deformations

In the previous examples, geometric nonlinearity has been used in order to take into account buckling behavior. In the following example, another interesting application is presented which emphasizes the influence of the chosen prescribed displacement on the outcome of optimization. We investigate the optimization of a clamped beam domain.

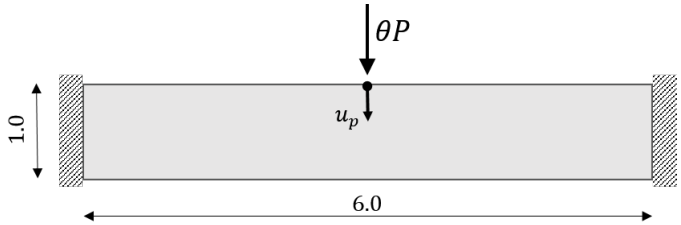

Figure 15: Optimizing for various global prescribed deformations – Geometry of the design domain, applied load and prescribed displacement.

The geometry of the design domain, the applied load and the prescribed displacement are shown in Fig. 15, and the ground structure is shown in Fig. 16a. A symmetric design is sought, therefore

the design domain consists of two symmetric halves each based on a grid of 4×6 hinges that is connected with all possible bars including overlapping bars. Horizontal overlapping bars that cross both halves were added to the connection between the two symmetric parts. The total number of bars is 540 and each bar is divided to two co-rotational beam elements, giving 1752 analysis DOF and 272 design variables.

In this example, the optimization is repeated for various magnitudes of the prescribed displacement. In addition, a solution without any geometric nonlinearity is generated for the sake of comparison. For generating the linear solution, a linear beam element was used and only global imperfection was applied. When solving for various prescribed displacements, the co-rotational beam element was used and both types of imperfections were applied. Global imperfection of camber shape with 0.1 in vertical and horizontal directions, were used here to induce chain instability; and local imperfections of 1% were applied to induce Euler buckling. Formulation (MaxF) was implemented with a given volume of $V^* = 0.2$; $A_{max} = 6.7 \cdot 10^{-2}$ and $A_{min} = 6.7 \cdot 10^{-8}$. A move limit of 0.1 was imposed on MMA design updates. The initial truss consists of uniform cross-sections of $2.67 \cdot 10^{-4}$ and satisfies the volume constraint with a value 0.2.

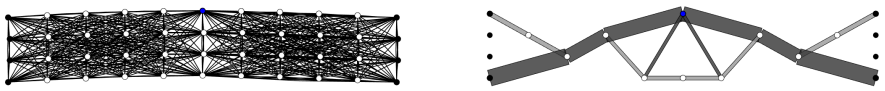

(a) Ground structure

(b) Optimized layout #1 with linear model

(c) Optimized layout #2 with $u_p = 1 \cdot 10^{-6}$

(d) Optimized layout #3 with $u_p = 1 \cdot 10^{-2}$

(e) Optimized layout #4 with $u_p = 5 \cdot 10^{-2}$

(f) Optimized layout #5 with $u_p = 1 \cdot 10^{-1}$

Figure 16: Optimization of a clamped truss structure for various magnitudes of the prescribed displacement.

The optimized layouts for different deformation scales are shown in Fig. 16b-f and are numbered 1-5 for convenient comparison. Results of the optimization are summarized in Table 3 and full response curves of all layouts are presented in Fig. 17 for two values of the prescribed displacement – $u_p = 1 \cdot 10^{-6}$ and $u_p = 1 \cdot 10^{-1}$. Due to the highly nonlinear behavior in large deformations, it was difficult to compute full response curves of layouts 1-3 using a standard displacement control scheme – this is in fact expected as these designs were optimized for small displacements. Therefore, an arc-length scheme was used to resolve the nonlinear analysis. In Fig. 17b, layout 1 is solved with local imperfection of 0.01 hence it buckles and so are layouts 2-4; and in Fig. 17a all layouts were solved using linear analysis in small prescribed deformation, without local imperfection, and

it can be seen that the maximum load-bearing capacity obtained in layout 1.

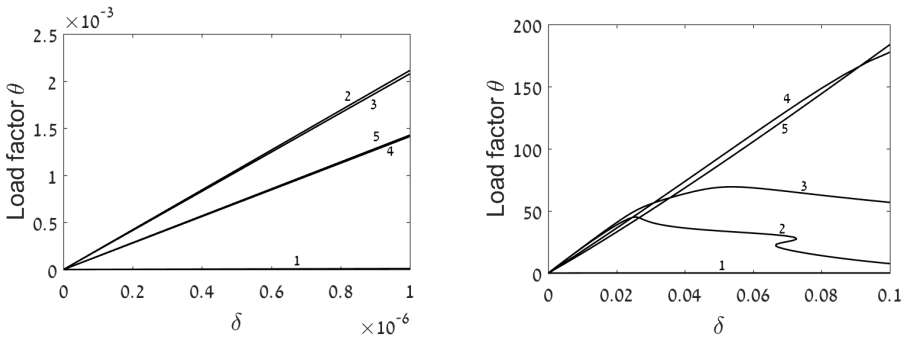

(a) Small prescribed displacement

(b) Large prescribed displacement

Figure 17: Full nonlinear response curves of the optimized designs of a clamped truss structure.

Table 3: Optimization of a clamped truss structure for various magnitudes of the prescribed displacement

Layout	Analysis	u_p	θ (initial)	θ (optimized)	Design iterations
1	Linear	-	-	-	-
2	Non-linear	$1 \cdot 10^{-6}$	$1.892 \cdot 10^{-4}$	$21.12 \cdot 10^{-4}$	35
3	Non-linear	$1 \cdot 10^{-2}$	$2.116 \cdot 10^{0}$	$20.69 \cdot 10^{0}$	100
4	Non-linear	$5 \cdot 10^{-2}$	$2.146 \cdot 10^{0}$	$92.82 \cdot 10^{0}$	214
5	Non-linear	$1 \cdot 10^{-1}$	$2.579 \cdot 10^{0}$	$183.7 \cdot 10^{0}$	200

A comparison between the optimized layouts clearly reveals the influence of the prescribed displacement on the nature of the optimized layout. Layouts obtained with small prescribed displacements contain long compressed bars, whereas under large displacements the optimization procedure generates layouts with long tensioned bars and short compressed bars. Also in this example, it is found that Euler buckling is imposed in compressed members of all the optimized layouts which were examined for the optimized load bearing capacity. As the magnitude of the prescribed displacement increases, the dominant load path switches from compression to tension, as can be seen by comparing Fig. 16c,d to Fig. 16e,f. This demonstrates the potential of the proposed formulation to be utilized not only for accounting for buckling, but also for including geometric non-linearity in the optimal design in general. In cases where nonlinear response is desired, or if the structure should maintain its stability also under large deformations, then the prescribed displacement can be chosen accordingly and optimization will lead to optimized and safe designs, based on the full non-linear analysis. Similar conclusions were deduced by (Lindgaard and Dahl, 2013) where optimal design of snap-through problems at a high load level lead to tension loaded structures and snap-through buckling was avoided.

6 Conclusions and future work

An approach capable of accounting for all buckling phenomena in truss optimization was presented in this paper. In the proposed optimization problem formulation, buckling is implicitly taken into account using a geometric nonlinear analysis, instead of imposing a large number of constraints. Several demonstrative examples and comparisons to benchmark results from the literature, show that the proposed approach is able to capture all buckling phenomena in trusses, namely global buckling, Euler buckling and chain stability, that results from the use of the ground structure approach. In addition, it is shown that the proposed formulation can avoid difficulties arising when imposing buckling constraints, such as the singularity of optimal solutions. A possible limitation is that optimization is driven by the end compliance objective, while for statically indeterminate optimized designs this objective may not capture all internal buckling occurrences – however this phenomenon was not encountered in the test cases.

It is evident that most of the computational effort in this approach is invested in computing the full geometric non-linear response, especially for non-stable intermediate designs. On the other hand, avoiding a large number of buckling constraints can simplify the solution of the nonlinear optimization problem. It is important to point out that the final topology is achieved in a relatively small number of design iterations, whereas most of the subsequent iterations are performed in order to remove overlapping bars. The choice of local and global imperfections has a significant effect on the results of the optimization procedure and on the types of buckling that are avoided in the optimized design. Furthermore, assuming non-consistent imperfections may lead to non-optimized layouts and cause convergence difficulties in the non-linear analysis.

In the current study, a well-established geometric non-linear beam finite element has been used successfully for capturing buckling. Future work will focus on enhancing the finite element model; improving the computational efficiency; further investigating the effect of choosing various imperfections; considering shape optimization of nodes positions; and accounting for stress constraints in a similar approach based on material nonlinearities, see (Amir, 2016) in the context of continuum topology optimization. Imperfections have been assumed according to the first buckling mode or deformations of the initial design only, and in some examples, bifurcation buckling was noticed within the optimization process, though not in the final design. This highlights an attractive extension that can be to consider various imperfections and optimizing the buckling resistance for the worst case, following Lindgaard et al. (2010), with emphasis on buckling mode-switching and imperfection sensitivity. Finally, the current formulation leads to a continuous distribution of cross-section areas. Therefore, we intend to enhance the applicability of this approach by adding practical considerations such as choosing standard cross-sections for bars or limiting the number of bars at connections. This can be achieved by penalizing continuous variables.

7 Acknowledgments

This work was funded by the European Commission Research Executive Agency, grant agreement PCIG12-GA-2012-333647. The financial support is gratefully acknowledged.

References

W. Achtziger. Local stability of trusses in the context of topology optimization. Part I: Exact modelling. Structural Optimization, 17(4):235–246, 1999. ISSN 09344373. doi: 10.1007/s001580050056.

O. Amir. Stress-constrained continuum topology optimization: a new approach based on elastoplasticity. Structural and Multidisciplinary Optimization, pages 1–22, 2016. ISSN 1615-147X. doi: 10.1007/s00158-016-1618-8.

J.-L. Batoz and G. Dhatt. Incremental Displacement Algorithms for Nonlinear Problems. Short Communications, 14(8):1262–1267, 1979. ISSN 0029-5981. doi: 10.1002/nme.1620140811.

A. Beghini, L. L. Beghini, and W. F. Baker. Applications of Structural Optimization in Architectural Design. Structures Congress 2013, pages 2499–2507, 2013. doi: 10.1061/9780784412848.218. URL http://ascelibrary.org/doi/abs/10.1061/9780784412848.218.

T. Belytschko and L. W. Glaum. Applications of higher order corotational stretch theories to nonlinear finite element analysis. Computers and Structures, 10(1-2):175–182, 1979. ISSN 00457949. doi: 10.1016/0045-7949(79)90085-3.

T. Belytschko and B. J. Hsieh. Non–linear transient finite element analysis with convected co–ordinates. International Journal for Numerical Methods in Engineering, 7(3):255–271, 1973. ISSN 0029-5981. doi: 10.1002/nme.1620070304.

A. Ben-Tal, F. Jarre, and M. Kočvara. Optimal design of trusses under a nonconvex global buckling constraint. Optimization and Engineering, 1:189–213, 2000. doi: 10.1023/A:1010091831812. URL http://link.springer.com/article/10.1023/A:1010091831812.

M. P. Bendsoe and O. Sigmund. Topology Optimization: Theory, Methods, and Applications. Springer Science & Business Media, 2003.

K. Besserud, N. Katz, and A. Beghini. Structural emergence: Architectural and structural design collaboration at SOM. Architectural Design, 83(2):48–55, 2013. ISSN 00038504. doi: 10.1002/ad.1553.

T. Buhl, C. Pedersen, and O. Sigmund. Stiffness Design of Geometrically Nonlinear Structures Using Topology Optimization. Structural and Multidisciplinary Optimization, 19:93–104, 2000. ISSN 1615-147X. doi: 10.1007/s001580050089.

S. Çarbas and M. P. Saka. Optimum Design of Single Layer Network Domes Using Harmony Search Method. Asian journal of Civil Engineering, 10(1):97–112, 2009.

S. Çarbas and M. P. Saka. Optimum topology design of various geometrically nonlinear latticed domes using improved harmony search method. Structural and Multidisciplinary Optimization, 45(3):377–399, 2012. ISSN 1615147X. doi: 10.1007/s00158-011-0675-2.

M. Crisfield. Nonlinear finite element analysis of solids and structures. Volume 1: Essentials. Wiley, New York, NY (United States), dec 1991. URL `http://www.osti.gov/scitech/biblio/226942`.

J. D. Deaton and R. V. Grandhi. A survey of structural and multidisciplinary continuum topology optimization: Post 2000. Structural and Multidisciplinary Optimization, 49(1):1–38, 2014. ISSN 1615147X. doi: 10.1007/s00158-013-0956-z.

B. Descamps and R. Filomeno Coelho. The nominal force method for truss geometry and topology optimization incorporating stability considerations. International Journal of Solids and Structures, 51(13):2390–2399, 2014. ISSN 00207683. doi: 10.1016/j.ijsolstr.2014.03.003.

P. Dombernowsky and A. Sondergaard. Three-dimensional topology optimisation in architectural and structural design of concrete structures. In Proceedings of the International Association for Shell and Spatial Structures (IASS) Symposium 2009, Valencia, number October, pages 1066–1077, 2009.

X. Guo, G. Cheng, and K. Yamazaki. A new approach for the solution of singular optima in truss topology optimization with stress and local buckling constraints. Structural and Multidisciplinary Optimization, 22(5):364–372, 2001. ISSN 1615147X. doi: 10.1007/s00158-001-0156-0.

X. Guo, G. D. Cheng, and N. Olhoff. Optimum design of truss topology under buckling constraints. Structural and Multidisciplinary Optimization, 30(3):169–180, 2005. ISSN 1615147X. doi: 10.1007/s00158-004-0511-z.

R. T. Haftka and Z. Gürdal. Elements of structural optimization. Springer Science & Business Media, 2012.

M. Jalalpour, T. Igusa, and J. K. Guest. Optimal design of trusses with geometric imperfections: Accounting for global instability. International Journal of Solids and Structures, 48(21):3011–3019, 2011. ISSN 00207683. doi: 10.1016/j.ijsolstr.2011.06.020. URL `http://dx.doi.org/10.1016/j.ijsolstr.2011.06.020`.

M. Kegl, B. Brank, B. Harl, and M. Oblak. Efficient handling of stability problems in shell optimization by asymmetric worst-case' shape imperfection. International Journal for Numerical Methods in Engineering, 73:1197–1216, 2008.

U. Kirsch. On singular topologies in optimum structural design. Structural Optimization, 2(3):133–142, 1990. ISSN 09344373. doi: 10.1007/BF01836562.

M. Kočvara. On the modelling and solving of the truss design problem with global stability constraints. Structural and Multidisciplinary Optimization, 23(3):189–203, 2002. ISSN 1615147X. doi: 10.1007/s00158-002-0177-3.

T. Kwon, L. B.C., and L. W.J. an Approximation Technique for Design Sensitivity Analysis of the Critical Load in Non-Linear Structures. International Journal for Numerical Methods in Engineering, 45(12):1727–1736, 1999.

E. Lindgaard and J. Dahl. On compliance and buckling objective functions in topology optimization of snap-through problems. Structural and Multidisciplinary Optimization, 47(3):409–421, 2013. ISSN 1615147X. doi: 10.1007/s00158-012-0832-2.

E. Lindgaard and E. Lund. A unified approach to nonlinear buckling optimization of composite structures. Computers and Structures, 89(3-4):357–370, 2011. ISSN 00457949. doi: 10.1016/j.compstruc.2010.11.008. URL http://dx.doi.org/10.1016/j.compstruc.2010.11.008.

E. Lindgaard, E. Lund, and K. Rasmussen. Nonlinear buckling optimization of composite structures considering "worst" shape imperfections. International Journal of Solids and Structures, 47(22-23):3186–3202, 2010. ISSN 00207683. doi: 10.1016/j.ijsolstr.2010.07.020. URL http://dx.doi.org/10.1016/j.ijsolstr.2010.07.020.

K. Mela. Resolving issues with member buckling in truss topology optimization using a mixed variable approach. Structural and Multidisciplinary Optimization, 50(6):1037–1049, 2014. ISSN 16151488. doi: 10.1007/s00158-014-1095-x.

S. Mostafavi, M. M. Beltran, and N. Biloria. Performance Driven Design and Design Information Exchange. Proceedings of the 31st International Conference on Education and research in Computer Aided Architectural Design in Europe, eCAADe 2013, 2:117–126, 2013.

H. Noguchi and T. Hisada. Sensitivity analysis in post-buckling problems of shell structures. Computers and Structures, 47(4-5):699–710, 1993. ISSN 00457949. doi: 10.1016/0045-7949(93)90352-E.

J. S. Park and K. K. Choi. Design Sensitivity Analysis of Critical Load Factor for Nonlinear Structural Systems. Computers & Structures, 36(5), 1990.

C. B. W. Pedersen. Topology optimization of 2D-frame structures with path-dependent response. International Journal for Numerical Methods in Engineering, 57(10):1471–1501, 2003. ISSN 00295981. doi: 10.1002/nme.787.

N. L. Pedersen and A. K. Nielsen. Optimization of practical trusses with constraints on eigenfrequencies, displacements, stresses, and buckling. Structural and Multidisciplinary Optimization, 25(5-6):436–445, 2003. ISSN 1615147X. doi: 10.1007/s00158-003-0294-7.

G. Rozvany. Difficulties in truss topology optimization with stress, local buckling and system stability constraints. Structural Optimization, 11(3-4):213–217, 1996. doi: 10.1007/BF01376857.

M. P. Saka. Optimum topological design of geometrically nonlinear single layer latticed domes using coupled genetic algorithm. Computers and Structures, 85(21-22):1635–1646, 2007. ISSN 00457949. doi: 10.1016/j.compstruc.2007.02.023.

M. P. Saka. Optimum Geometry Design of Geodesic Domes Using Harmony Search Algorithm. Advances in Structural Engineering, 10(6):595–606, 2009. ISSN 1369-4332. doi: 10.1260/136943307783571445.

O. Sigmund and K. Maute. Topology optimization approaches: A comparative review. Structural and Multidisciplinary Optimization, 48(6):1031–1055, 2013. ISSN 1615147X. doi: 10.1007/s00158-013-0978-6.

A. Søndergaard, O. Amir, and M. Knauss. Topology Optimization and Digital Assembly of Advanced Space-Frame Structures. Acadia, pages 367–378, 2013.

A. Søndergaard, O. Amir, P. Eversmann, L. Piskorec, F. Stan, F. Gramazio, and M. Kohler. Topology Optimization and Robotic Fabrication of Advanced Timber Space-Frame Structures. Robotic Fabrication in Architecture, Art and Design 2016, (2016):190–203, 2016. ISSN 1098-6596. doi: 10.1007/978-3-319-04663-1. URL http://link.springer.com/10.1007/978-3-319-04663-1.

L. L. Stromberg, A. Beghini, W. F. Baker, and G. H. Paulino. Topology optimization for braced frames: Combining continuum and beam/column elements. Engineering Structures, 37:106–124, 2012. ISSN 01410296. doi: 10.1016/j.engstruct.2011.12.034. URL http://dx.doi.org/10.1016/j.engstruct.2011.12.034.

K. Svanberg. The method of moving asymptotesa new method for structural optimization. International Journal for Numerical Methods in Engineering, 24(2):359–373, 1987. ISSN 00295981. doi: 10.1002/nme.1620240207. URL http://onlinelibrary.wiley.com/doi/10.1002/nme.1620240207/abstract.

A. J. Torii, R. H. Lopez, and L. F. F. Miguel. Modeling of global and local stability in optimization of truss-like structures using frame elements. Structural and Multidisciplinary Optimization, 51 (6):1187–1198, 2015. ISSN 16151488. doi: 10.1007/s00158-014-1203-y.

A. Tyas, M. Gilbert, and T. Pritchard. Practical plastic layout optimization of trusses incorporating stability considerations. Computers and Structures, 84(3-4):115–126, 2006. ISSN 00457949. doi: 10.1016/j.compstruc.2005.09.032.

G. Wempner. Finite elements, finite rotations and small strains of flexible shells. International Journal of Solids and Structures, 5(15):117–153, 1969. ISSN 00207683. doi: 10.1016/0020-7683(69)90025-0. URL http://dx.doi.org/10.1016/0020-7683(69)90025-0.

C. Wu and J. Arora. Design sensitivity analysis of non-linear buckling load*. Computational Mechanics, 3(2):129–140, 1988.

M. Zhou. Difficulties in truss topology optimization with stress and local buckling constraints. Structural Optimization, 11(2):134–136, 1996. ISSN 0934-4373. doi: 10.1007/BF01376857.